Supplementary Material
Altered White Matter Organization in the TUBB3 E410K Syndrome
P. Ellen Grant et al, Cerebral Cortex 2018

A. Supplementary Methods

a. Cognitive/developmental and language assessments
b. Region of Interest (ROI) placement for tract segmentation

B. Supplementary Results

a. Subject 4

C. Supplementary Figures and Figure Legends

Supplementary Fig. 1. Genetics of Subject 4 and Structural MRI of Subjects 3 and 4
Supplementary Fig. 2. Effect of noise on tractography
Supplementary Fig. 3A. Corticospinal tracts (CST), medial lemniscus (ML) – Pediatric Controls
Supplementary Fig. 3B. Corticospinal tracts (CST), medial lemniscus (ML) – Adult Controls
Supplementary Fig. 4A. Corpus Callosum (CC) – Pediatric Controls
Supplementary Fig. 4B. Corpus Callosum (CC) – Adult Controls
Supplementary Fig. 5A. Dorsal Language Network (DLN) – Pediatric Controls
Supplementary Fig. 5B. Dorsal Language Network (DLN) – Adult Controls
Supplementary Fig. 6A. Ventral Language Network (VLN) – Pediatric Controls
Supplementary Fig. 6B. Ventral Language Network (VLN) – Adult Controls
Supplementary Fig. 7A. Cingulum (Cing) – Pediatric Controls
Supplementary Fig. 7B. Cingulum (Cing) – Adult Controls

D. Supplementary Tables

Supplementary Table 1. Group comparisons of whole brain diffusion measures
Supplementary Table 2. Statistical results for the group comparisons of mean and variance of FA values between pediatric and adult control groups
Supplementary Table 3. Statistical results for the group comparisons of mean and variance of FA values between pediatric and adult subjects in TUBB3 E410K group

E. Supplementary References

A. Supplementary Methods

a. Cognitive/developmental and language assessments

Intellectual/Developmental functioning was assessed using Stanford-Binet Intelligence Scale – Fifth Edition (SB5) (Roid GH 2003) or the Wechsler Intelligence Scale for Children - Fourth Edition (WISC-IV) (Wechsler D 2003). The Mullen Scales of Early Learning (MSEL) (Mullen EM 1995), a developmental measure for infants/toddlers, was used to obtain a cognitive index. Language was assessed using the Oral and Written Language Scales (OWLS) (Carrow-Woolfolk E 1995) and Clinical Evaluation of Language Fundamentals – Fourth Edition (CELF-4) (Semel E et al. 2003). Adaptive functioning was assessed using the Adaptive Behavior Assessment System – Second Edition (ABAS-II) (Harrison PL and T Oakland 2003), Vineland Adaptive Behavior Scale (VABS) (Sparrow SS et al. 1984), or Vineland Adaptive Behavior Scale – Second Edition (VABS-II) (Sparrow S et al. 2005). ASD diagnostic measures and behavioral questionnaires included the Autism Diagnostic Interview-Revised (ADI-R) (Le Couteur A et al. 1989; Lord C et al. 1994), Autism Diagnostic Observation Schedule (ADOS) (Lord C et al. 2000), Social Responsiveness Scale (SRS) (Constantino JN 2002), and Social Communication Questionnaire (SCQ) (Rutter M et al. 2003). Emotional and behavioral functioning were assessed using the Child Behavior Checklist (CBCL) (Achenbach TM and LA Rescorla 2001). Other measures that were administered to some individuals included: a) Assessment of anxiety/depression: Multidimensional Anxiety Scale for Children (MASC)(March JS 1997), Children's Depression Inventory (CDI) (Kovacs M 1992), Beck Depression Inventory-II (BDI-II) (Beck AT et al. 1996), Revised Child Anxiety and Depression Scale (RCADS) (Chorpita BF et al. 2000; Chorpita BF et al. 2005); b) Assessment of attention: Conners' Parent Rating Scale-Revised Short version (Conners KC 2008), Strengths and Weaknesses of ADHD Symptoms and Normal Behavior Rating Scale (SWAN) (Swanson JM et al. 2012); and c) Assessment of executive functions: Behavior Rating Inventory of Executive Function (BRIEF) (Gioia GA et al. 2000).

b. Region of Interest (ROI) placement for manual tract segmentation

Projection Fibers

Corticospinal tract (CST) and Medial Lemniscus (ML), Fig. 3. and Supplementary Figs. 3A and 3B. Three ROIs were used to identify descending fibers likely to belong to the CST. The first ROI was placed in the ipsilateral cerebral peduncle, which was identified anatomically on the axial plane on the ADC map. The second one was placed in the anterior pons and the third in the posterior pons; both pontine regions were visualized on the axial plane on the color FA map as blue regions (arrows in Fig. 3, row 1 column A) (Kumar et al., 2009; Radmanesh et al., 2015; Weiss et al., 2015; Niu et al., 2016). To identify ML ascending fibers, we used the same three ROIs as for the CST but the cerebral peduncle ROI was an exclusion ROI ("no part"), so only the fibers that went through the anterior or posterior pons but not the cerebral peduncle were considered part of the ML. In this way we explored potential misguidance of descending and ascending fibers by classifying CST fibers as those that coursed superior-inferiorly in the pons and passed through the cerebral peduncle, and ML fibers as those that coursed superior-inferiorly in the pons but did not pass through the cerebral peduncle.

Interhemispheric Fibers

Corpus Callosum (CC), Fig. 4 and Supplementary Figs. 4A and 4B. The CC was segmented from the color FA map using three mid-sagittal slices on which the CC was visible. Exclusion masks were used to remove fibers belonging to the fornix and the CST. For the TD controls, the five regions of the CC were automatically segmented using Freesurfer (surfer.nmr.mgh.harvard.edu), which measures the distance between the anterior CC and the posterior CC on the midsagittal slice of the CC and divides the distance

into five equal segments. The segmented regions were visually checked for accuracy and required little manual editing to clean up the CC boundaries. For the TUBB3 E410K participants, the segmentation measurements were performed semi-automatically on each of the data sets to obtain five equal segments of the CC because automatic segmentation with Freesurfer fails. These five segments were used as ROI masks in the tract reconstruction program (TrackVis.org) to create Fig. 4 and Supplementary Figs. 4A and 4B, Columns A, C, and E. In both subjects and controls whole CC masks were also used to reconstruct tracts in 3DSlicer's (www.slicer.org) SlicerDMRI project (dmri.slicer.org) (Norton et al., 2017) to show the anatomical directions of the fiber tract segments, visualizing both the fiber and the ellipsoid direction of the fiber bundles in Fig. 4 and Supplementary Figs. 4A and 4B, Columns B and D.

Intrahemispheric Fibers

Dorsal Language Network (DLN), Fig. 5 and Supplementary Figs. 5A and 5B. The anatomy of the superior longitudinal fasciculus (DLN.ant) and arcuate fasciculus (DLN.long) is controversial (Dick AS and P Tremblay 2012). For the purposes of this study we used the "three segment" model proposed by Catani et al (Catani M et al. 2005), using a three region of interest approach as outlined in this publication. To segment the long segment (DLN.long; red), which describes the classical arcuate fasciculus, an ROI was placed in the axial plane at the level of the widest part of the corpus callosum. To segment the superior longitudinal fasciculus or anterior segment of the dorsal language network (DLN.ant; green), an ROI was placed in the anterior coronal plane immediately adjacent to the widest part of the corpus callosum. To segment the posterior segment (DLN.post; yellow) in the parietal lobe, an ROI was placed in the axial plane, posterior to ROI's for the DLN.long (red) and DLN.ant (green) segments (Forkel SJ et al. 2014).

Ventral Language Network (VLN), Fig. 6 and Supplementary Figs. 6A and 6B. To segment the VLN.IFOF (red), a single ROI was placed in the sagittal plane to identify the main stem (Hau J et al. 2016). To segment the VLN.ILF (green), a single ROI was placed in the anterior temporal lobe, just superior to the tip of the hippocampus (Catani M and M Thiebaut de Schotten 2008; Martino J and EM De Lucas 2014). To segment the uncinate fasciculus (VLN.UF; yellow), an ROI was placed in the coronal plane in the anterior temporal lobe and an exclusion ROI was placed in the coronal plane posterior to the elbow of the VLN.UF to remove closely passing VLN.ILF and VLN.IFOF fibers.

Cingulum (Cing), Fig. 7 and Supplementary Figs. 7A and 7B. Cingulum fibers were segmented following the procedure outlined in Catani and de Schotten (Catani M and M Thiebaut de Schotten 2008), with the addition of an exclusion mask to remove CC fibers that run in close proximity to the fronto-parietal portion of the cingulate bundle.

C. Supplementary Results

Clinical evaluation of Subject 4. Subject 4 was evaluated clinically at 8 years 3 months of age. He was born full-term following an uncomplicated pregnancy, and was treated medically for supraventricular tachycardia (SVT) from birth to 3 years of age. He has unilateral ptosis and bilaterally exotropic and hypotropic primary eye positions with limited vertical and horizontal eye movements, and small, sluggishly reactive pupils. He has midface hypoplasia and bilateral facial weakness. He has anosmia and, at birth, had been noted to have a small phallus consistent with hypogonadotropic hypogonadism. He had no history of stridor, vocal cord paralysis or respiratory distress, and had not developed signs or symptoms of peripheral neuropathy or cyclic vomiting. His family history is unremarkable.

D. Supplementary Figures and Figure Legends

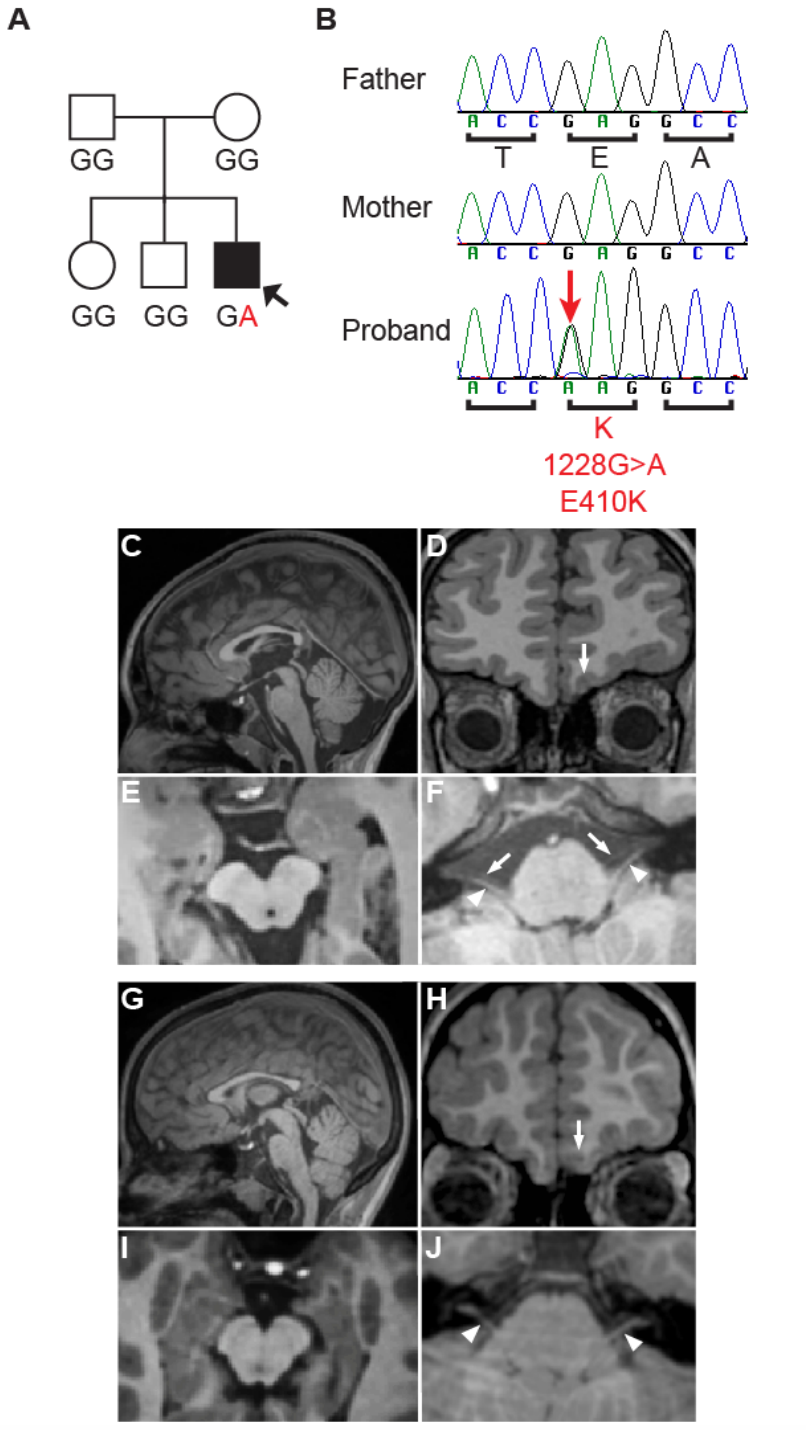

Supplementary Figure 1. Genetics of Subject 4 and Structural MRI of Subjects 3 and 4. (A) Schematic of subject 4's pedigree. Filled symbol = affected; arrow = proband. *TUBB3* nucleotide at position c.1228 is either wildtype (GG) or, in the proband, heterozygous for the *de novo* missense mutation that results in the E410K syndrome (GA). **(B)** Electropherograms of relevant *TUBB3* sequence from subject 4 (bottom) and his father and mother. The proband harbors a heterozygous 1228G>A missense mutation indicated by an arrow over his sequence. The mutation is absent in the DNA of his unaffected parents. **(C-J)** Representative volumetric T1-weighted MR images of the brains of subject 4 (C-F) and subject 3 (G-J). Midline sagittal views demonstrate thinning of the CC (C,G) with partial agenesis in subject 4 (C). Coronal views demonstrate absent olfactory bulbs and right olfactory sulci, and dysplastic left olfactory sulci (arrow, D, H). Axial views of the midbrain demonstrate absent oculomotor nerves (E, I) and axial views of the pons demonstrate vestibulocochlear nerves (arrowheads) but hypoplastic (arrow, F) or absent facial nerves (J).

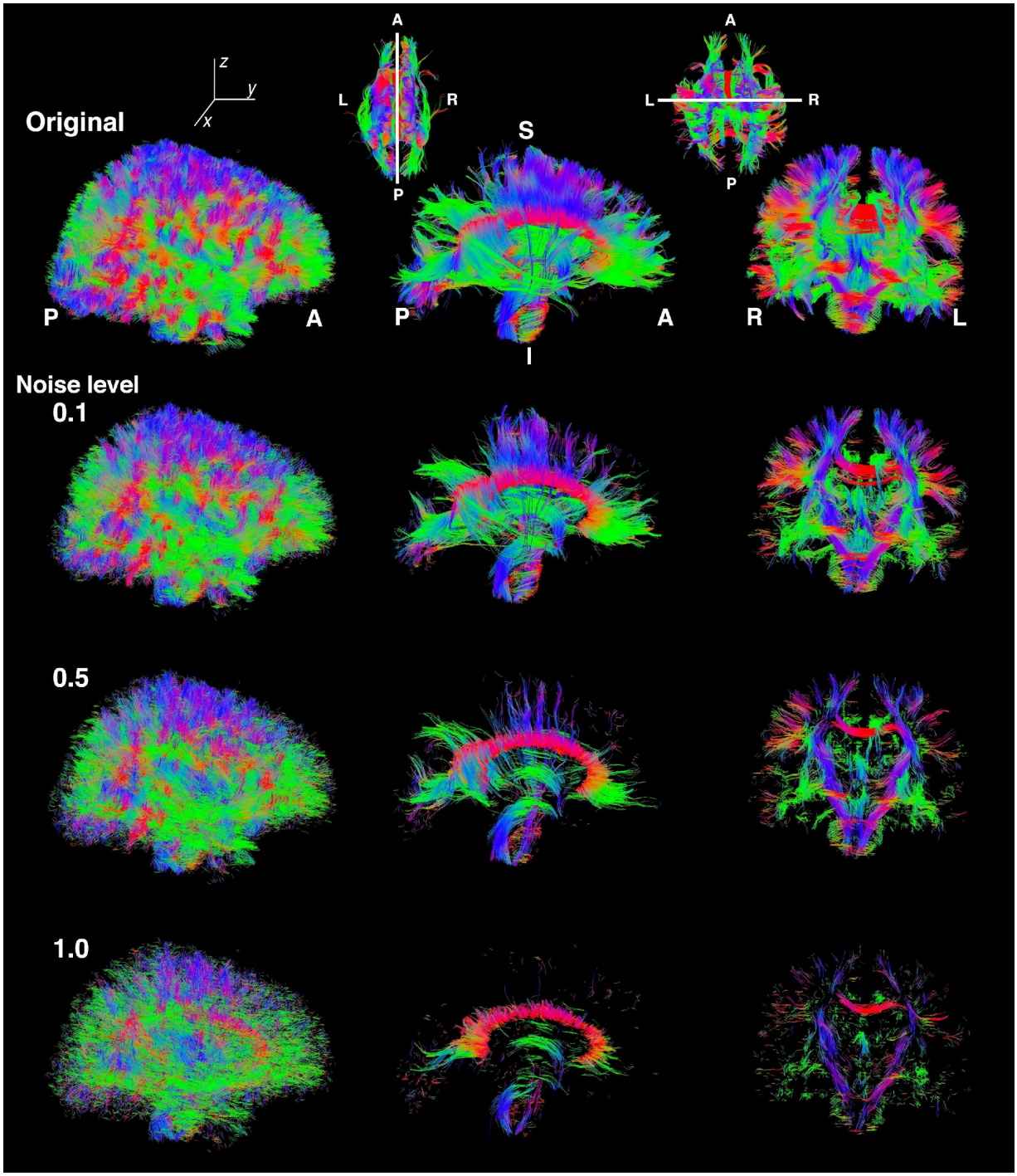

Supplementary Figure 2. Effect of noise on tractography. Gaussian white noise of mean 0 was added to the raw diffusion weighted images. The variance of noise was determined as 0.1, 0.5, and 1% of maximum intensity range, and then tracts were reconstructed. Whole brain fiber tracts (left column) and tracts filtered by *yz*- and *xz*-planes (middle and right column respectively) are shown for one adult control with different noise levels in each row. The direction of the fiber tracts is color-coded as per standard RGB convention for fiber direction, red corresponds to right/left, green corresponds to anterior/posterior, and blue corresponds to superior/inferior. L: left, R: right, A: anterior, P: posterior, S: superior, I: inferior.

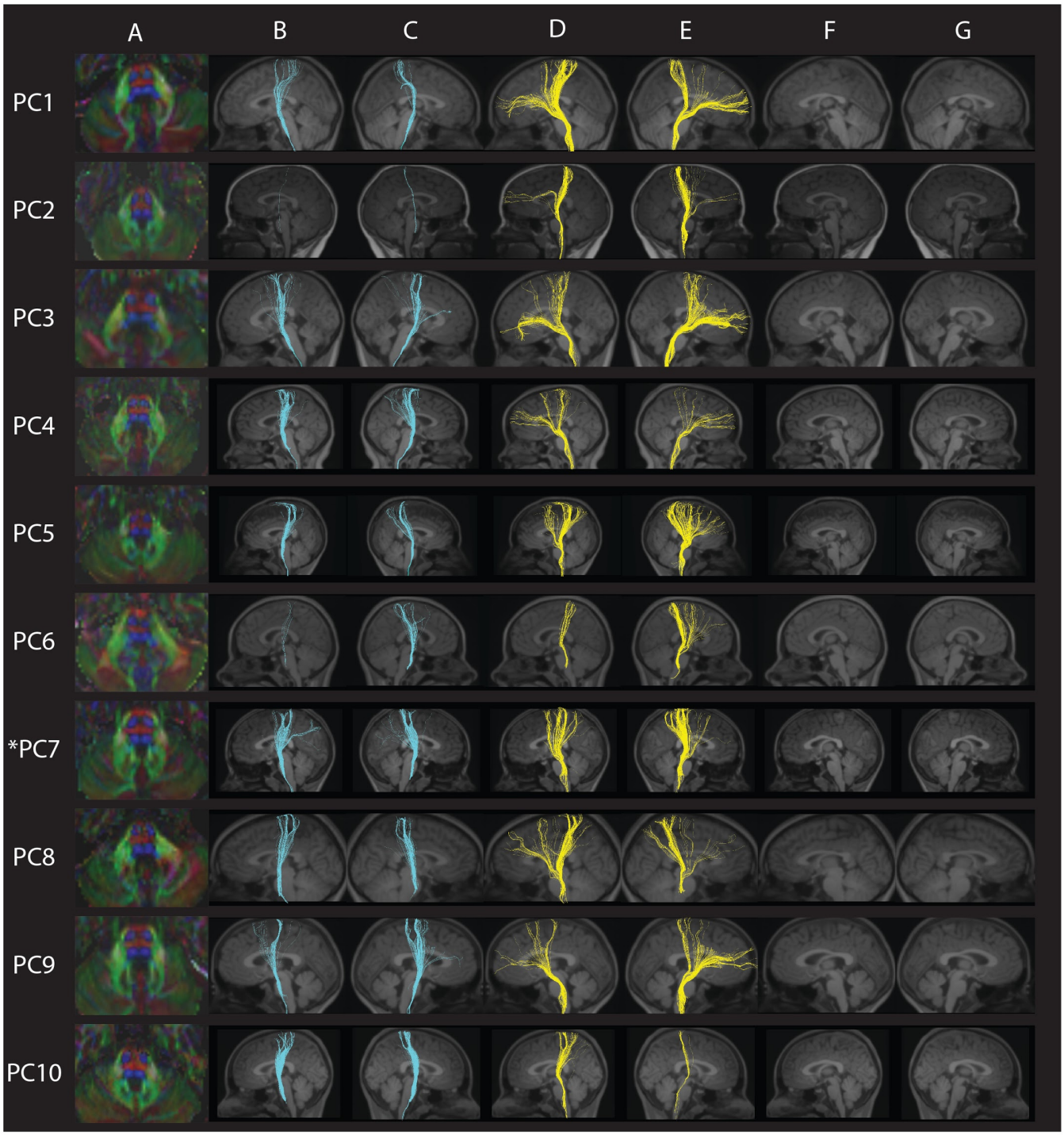

Supplementary Figure 3A. Corticospinal tracts (CST), medial lemniscus (ML) – Pediatric Controls, related to Figure 3. Each row represents images for a single individual. * Denotes pediatric control that also appears in Fig. 3. **Column A:** Axial view of the mid pons in FA color map. **Column B:** Left hemisphere showing the CST. **Column C:** Right hemisphere showing the CST. **Column D:** Left hemisphere showing the ML. **Column E:** Right hemisphere showing the ML. **Column F:** Absence of fibers evidenced by placing two inclusion ROIs; one in the left cerebral peduncle and the other in the ipsilateral posterior pons. **Column G:** Absence of fibers evidenced by placing two inclusion ROIs; one in the right cerebral peduncle and the other in the ipsilateral posterior pons.

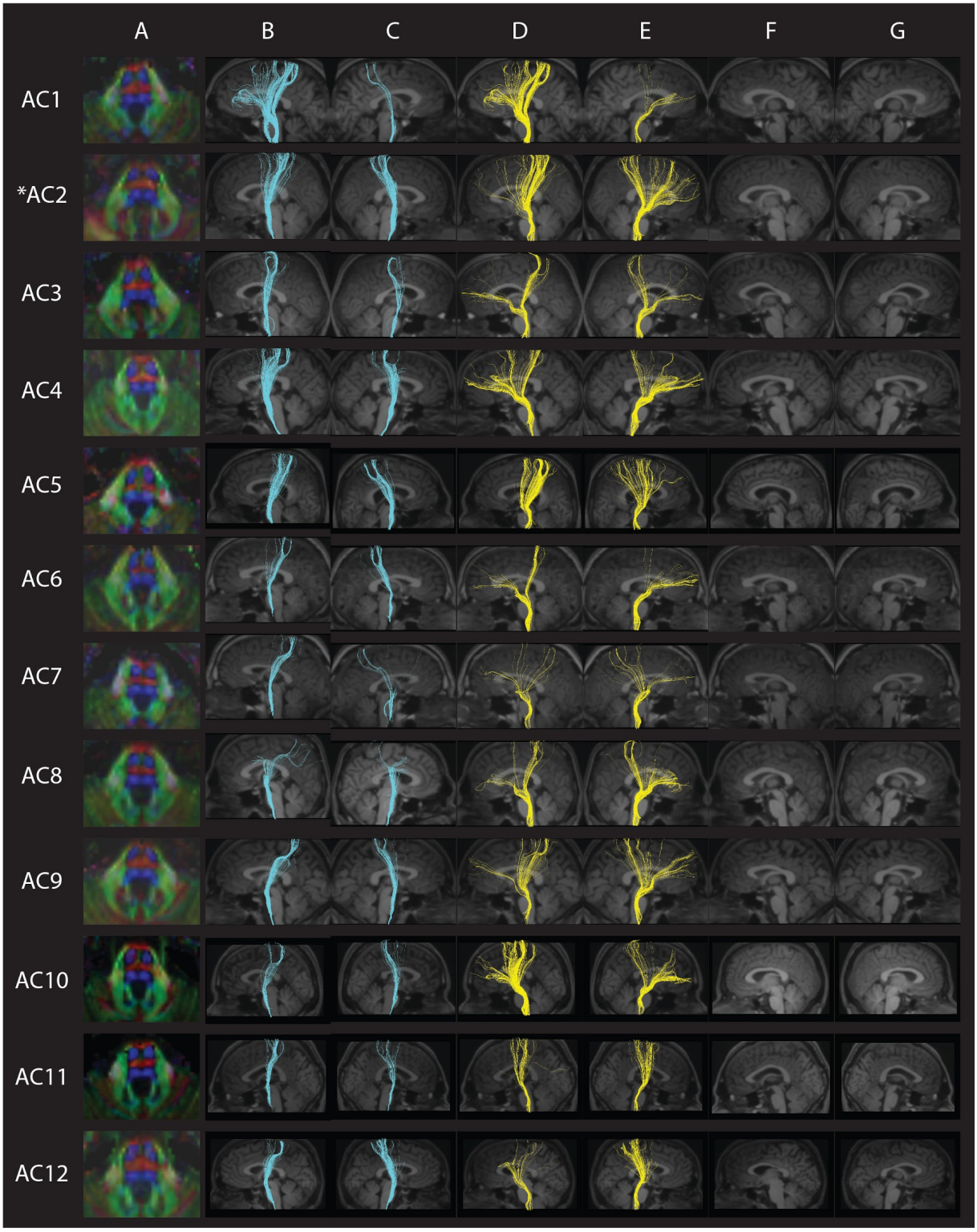

Supplementary Figure 3B. Corticospinal tracts (CST), medial lemniscus (ML) – Adult Controls, related to Figure 3. Each row represents images for a single individual. * Denotes adult control that also appears in Fig. 3. **Column A:** Axial view of mid pons in FA color map. **Column B:** Left hemisphere showing the CST. **Column C:** Right hemisphere showing the CST. **Column D:** Left hemisphere showing the ML. **Column E:** Right hemisphere showing the ML. **Column F:** Absence of fibers evidenced by placing two inclusion ROIs; one in the left cerebral peduncle and the other in the ipsilateral posterior pons. **Column G:** Absence of fibers evidenced by placing two inclusion ROIs; one in the right cerebral peduncle and the other in the ipsilateral posterior pons.

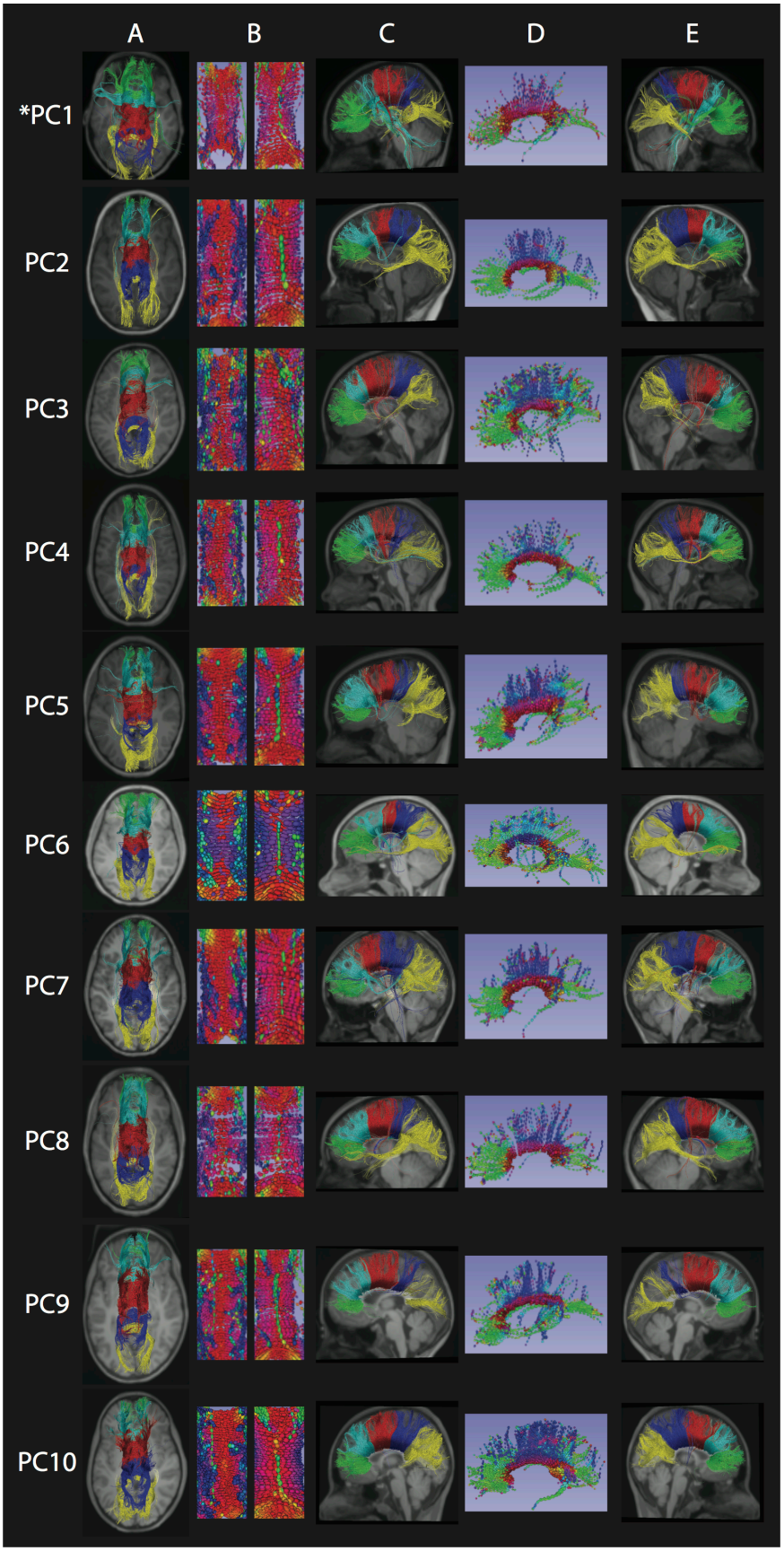

Supplementary Figure 4A. Corpus Callosum (CC) - Pediatric Controls, related to Figure 4. Each row represents images for a single individual. * Denotes pediatric control that also appears in Fig. 4. Note that the CC was divided in 5 different segments: green = anterior CC, turquoise = mid-anterior CC, red = central CC, dark blue = mid-posterior CC, yellow = posterior CC. **Column A:** Axial view of CC. **Column B:** Axial views – respectively superior and anterior – of CC, with ellipsoids showing orientation and organization of the fibers using standard RGB conventions for fiber direction; created with 3D Slicer via the Slicer DMRI Project (dmri.slicer.org) (Norton I et al. 2017). **Column C:** Left hemisphere showing the CC. **Column D:** Left hemisphere of CC created with 3D Slicer via the Slicer DMRI Project. **Column D:** Right hemisphere showing the CC.

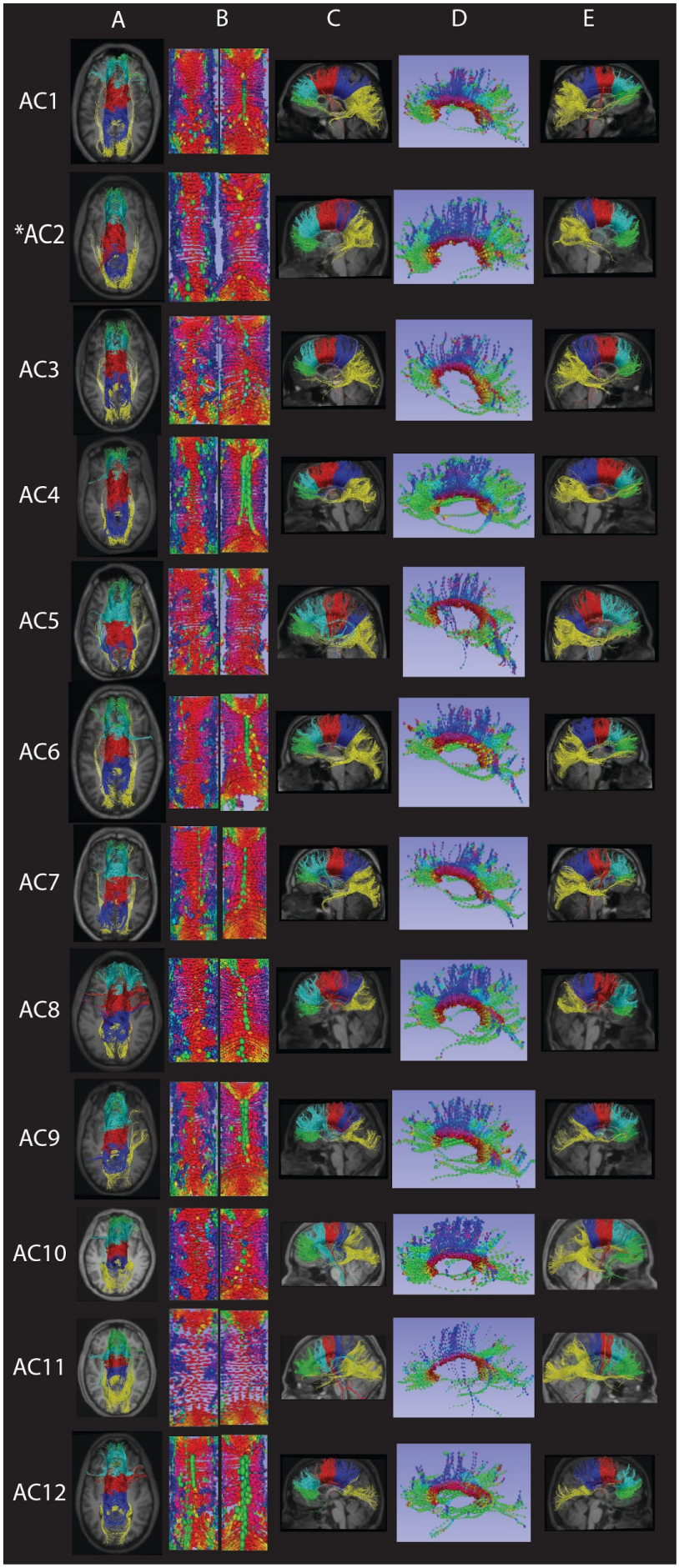

Supplementary Figure 4B. Corpus Callosum (CC) - Adult Controls, related to Figure 4. Each row represents images for a single individual. * Denotes adult control that also appears in Fig. 4. Note that the CC was divided in 5 different segments: green = anterior CC, turquoise = mid-anterior CC, red = central CC, dark blue = mid-posterior CC, yellow = posterior CC. **Column A:** Axial view of CC. **Column B:** Axial views – respectively superior and anterior – of CC, with ellipsoids showing orientation and organization of the fibers using standard RGB conventions for fiber direction; created with 3D Slicer via the Slicer DMRI Project (dmri.slicer.org) (Norton I et al. 2017). **Column C:** Left hemisphere showing the CC. **Column D:** Left hemisphere of CC created with 3D Slicer via the Slicer DMRI Project. **Column D:** Right hemisphere showing the CC.

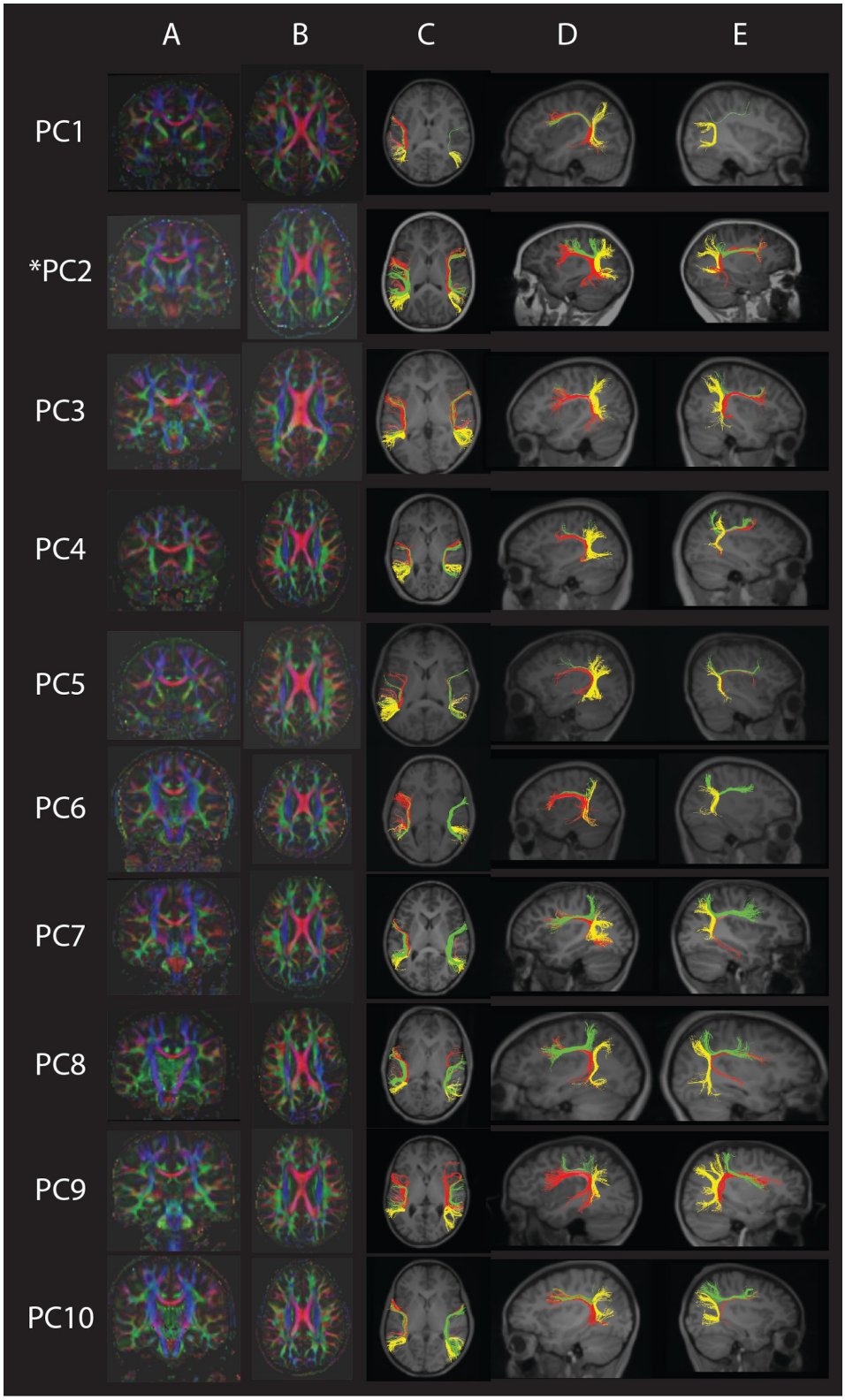

Supplementary Figure 5A. Dorsal Language Network (DLN) - Pediatric Controls, related to Figure 5. Each row represents images for a single individual. * Denotes pediatric control that also appears in Fig. 5. Note the three different tracts that compose the DLN: (1) Anterior segment (DLN.ant; green), (2) Long segment (DLN.long; red), and (3) Posterior segment (DLN.post; yellow). **Column A:** Coronal view of FA color map. **Column B:** Axial view of FA color map. **Column C:** Axial view of both hemispheres, showing bilateral DLN tracts. **Column D:** Left hemisphere showing the DLN. **Column E:** Right hemisphere showing the DLN.

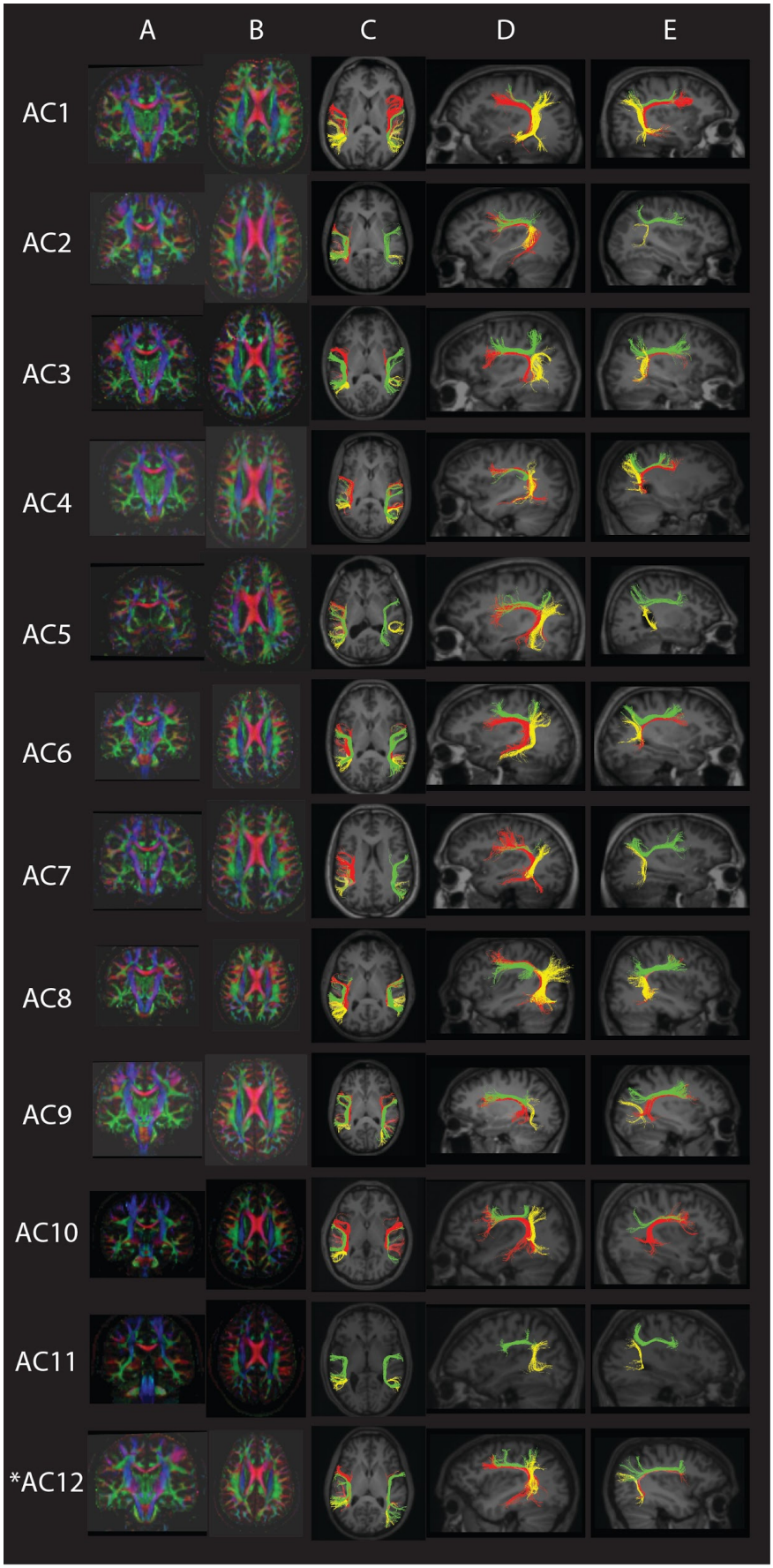

Supplementary Figure 5B. Dorsal Language Network (DLN) - Adult Controls, related to Figure 5. Each row represents images for a single individual. * Denotes adult control that also appears in Fig. 5. Note the three different tracts that compose the DLN: (1) Anterior segment (DLN.ant; green), (2) Long segment (DLN.long; red), and (3) Posterior segment (DLN.post; yellow). **Column A:** Coronal view of FA color map. **Column B:** Axial view of FA color map. **Column C:** Axial view of both hemispheres, showing bilateral DLN tracts. **Column D:** Left hemisphere showing the DLN. **Column E:** Right hemisphere showing the DLN.

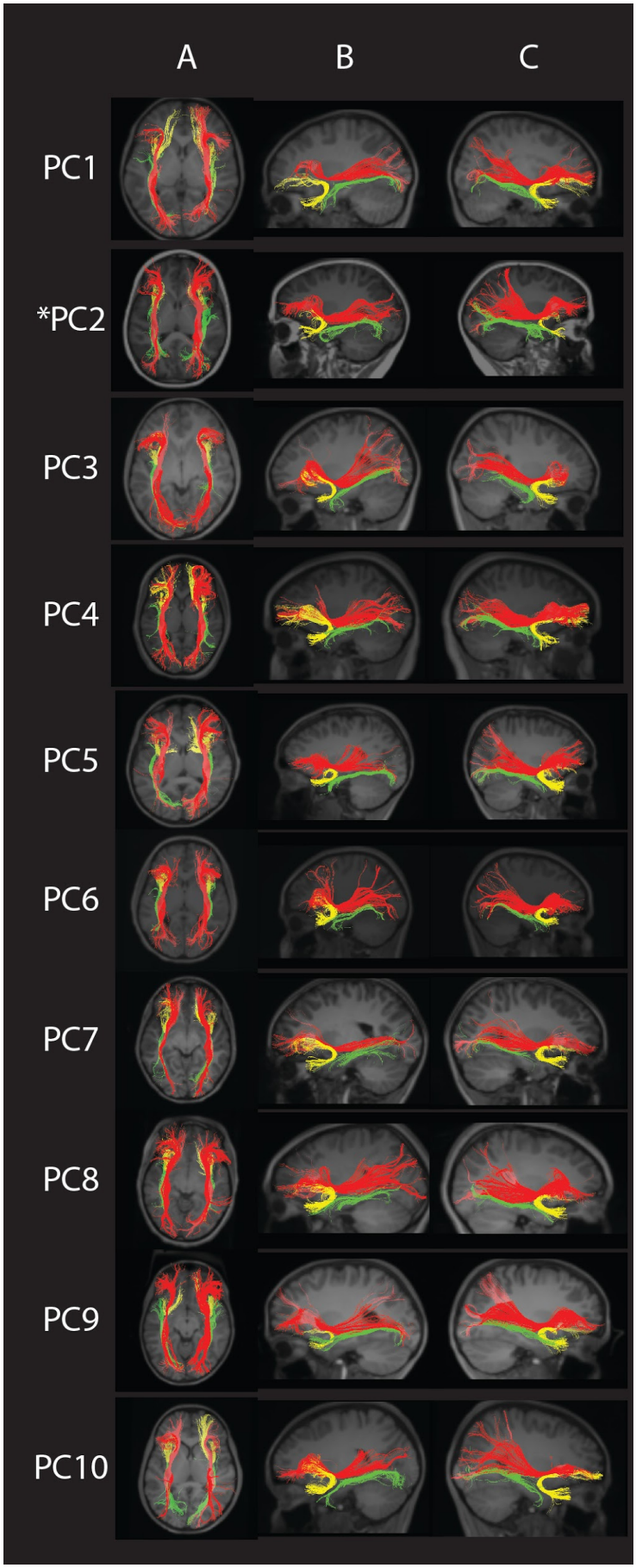

Supplementary Figure 6A. Ventral Language Network (VLN) – Pediatric Controls, related to Figure 6. Each row represents images for a single individual. * Denotes pediatric control that also appears in Fig. 6. Note the three different tracts that compose the VLN: (1) Inferior fronto-occipital fasciculus (VLN.IFOF; red), (2) Inferior longitudinal fasciculus (VLN.ILF; green), and (3) Uncinate fasciculus (VLN.UF; yellow). **Column A:** Axial view of both hemispheres, showing bilateral VLN. **Column D:** Left hemisphere showing the VLN. **Column E:** Right hemisphere showing the VLN.

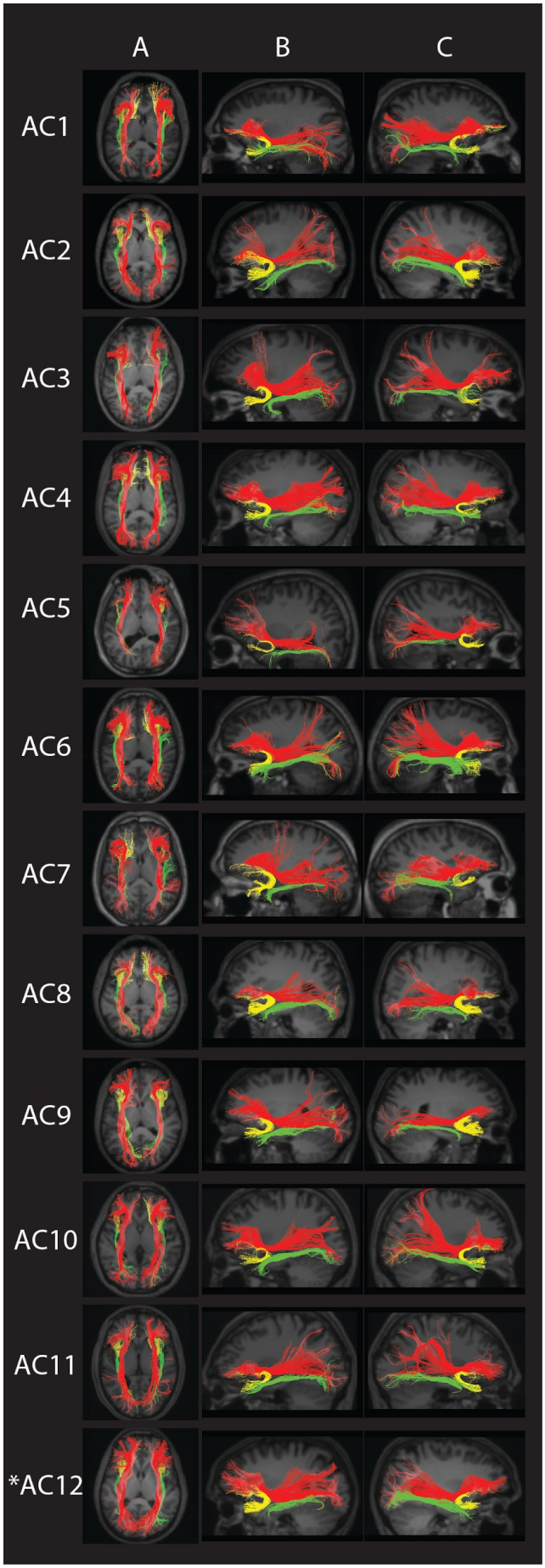

Supplementary Figure 6B. Ventral Language Network (VLN) – Adult Controls, related to Figure 6. Each row represents images for a single individual. * Denotes adult control that also appears in Fig. 6. Note the three different tracts that compose the VLN: (1) Inferior fronto-occipital fasciculus (VLN.IFOF; red), (2) Inferior longitudinal fasciculus (VLN.ILF; green), and (3) Uncinate fasciculus (VLN.UF; yellow). **Column A:** Axial view of both hemispheres, showing bilateral VLN. **Column D:** Left hemisphere showing the VLN. **Column E:** Right hemisphere showing the VLN.

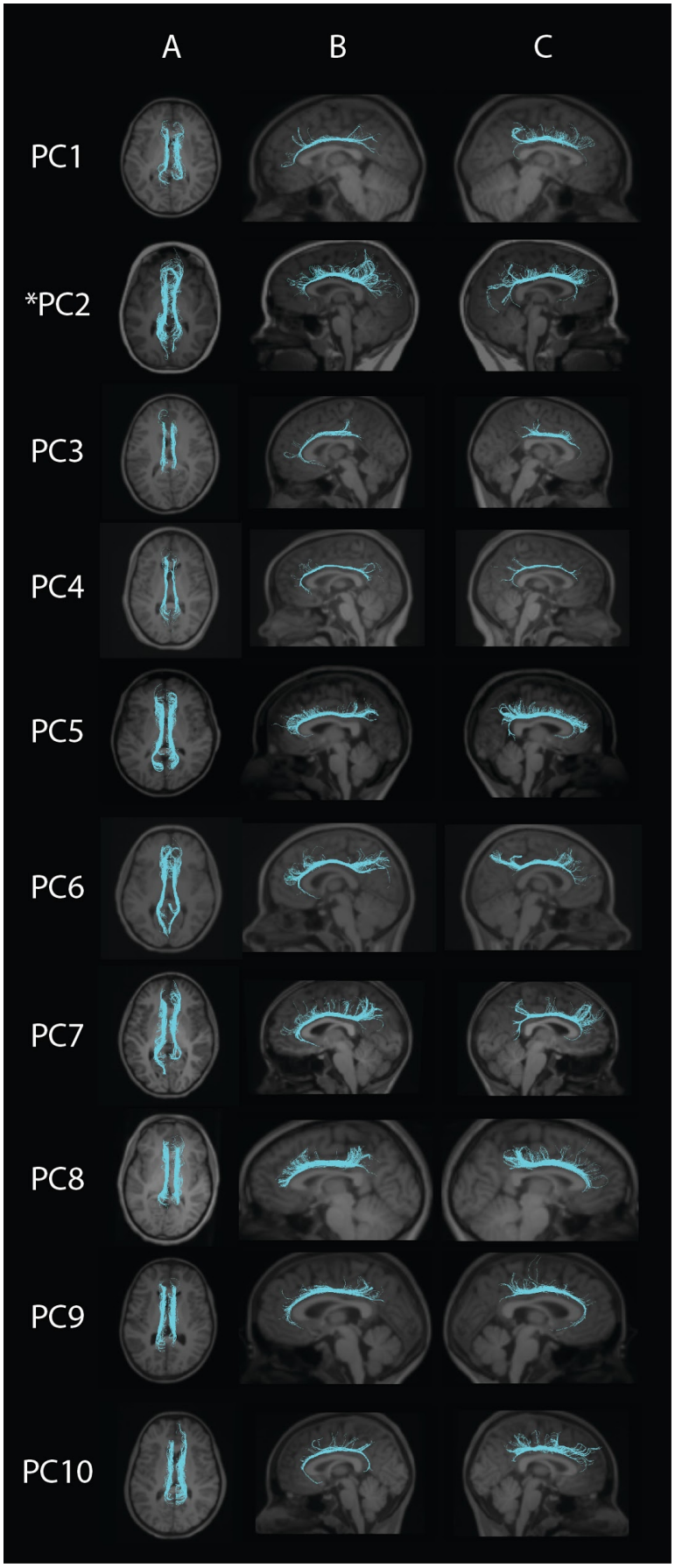

Supplementary Figure 7A. Cingulum – Pediatric Controls. related to Figure 7. Each row represents images for a single individual. * Denotes pediatric control that also appears in Fig. 7. **Column A:** Axial view of both hemispheres, showing bilateral cingulum. **Column D:** Left hemisphere showing the cingulum. **Column E:** Right hemisphere showing the cingulum.

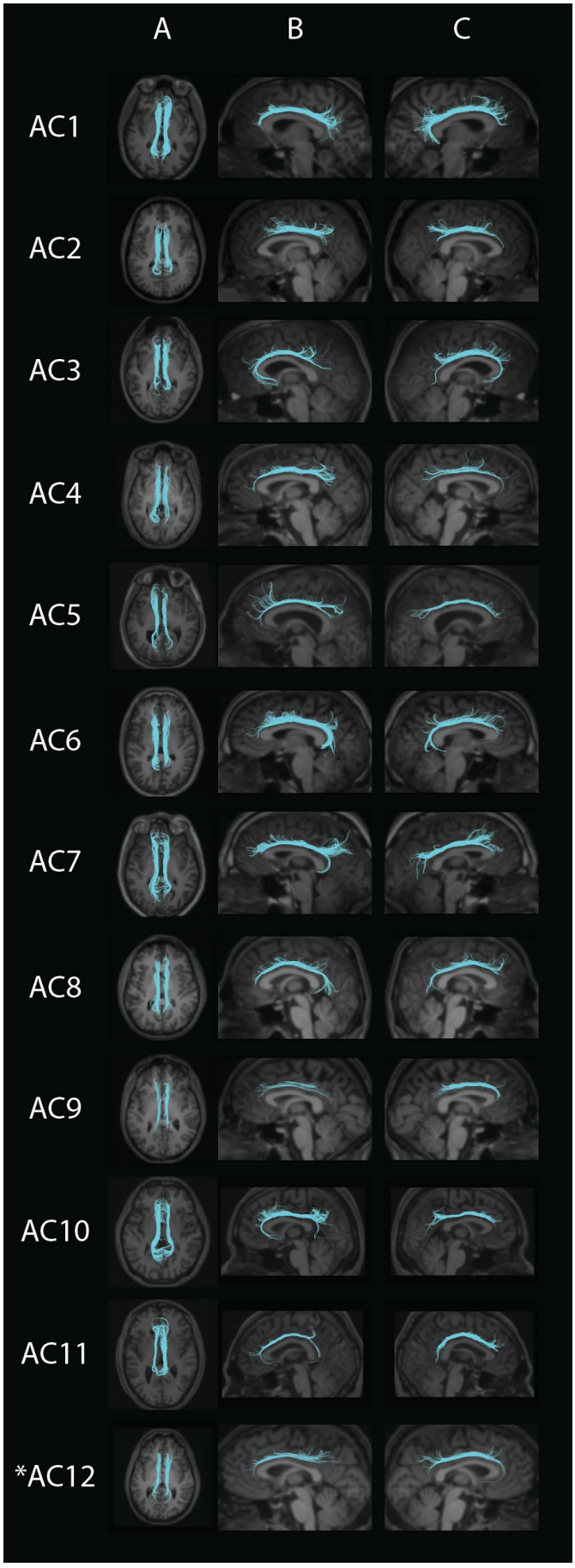

Supplementary Figure 7B. Cingulum – Adult Controls, related to Figure 7. Each row represents images for a single individual. * Denotes adult control that also appears in Fig. 7. **Column A:** Axial view of both hemispheres, showing bilateral cingulum. **Column D:** Left hemisphere showing the cingulum. **Column E:** Right hemisphere showing the cingulum.

D. Supplementary Tables

Supplementary Table 1. Statistical results for the group comparisons of whole brain diffusion measures

		TD	TUBB3 E410K	*p*
Pediatric	FA	0.397 (0.015)	0.370 (0.011) [0.357, 0.383, 0.365, 0.373]	0.014*
	MD ($\times 10^{-3}$)	0.788 (0.021)	0.830 (0.029) [0.789, 0.833, 0.843, 0.856]	0.036*
	RD ($\times 10^{-3}$)	0.615 (0.024)	0.664 (0.021) [0.635, 0.660, 0.677, 0.682]	0.008*
	AD ($\times 10^{-3}$)	1.130 (0.021)	1.165 (0.047) [1.097, 1.183, 1.175, 1.204]	0.142
Adult	FA	0.413 (0.020)	0.402 (0.010) [0.397, 0.397, 0.413]	0.233
	MD ($\times 10^{-3}$)	0.791 (0.023)	0.810 (0.037) [0.853, 0.791, 0.786]	0.448
	RD ($\times 10^{-3}$)	0.609 (0.026)	0.634 (0.030) [0.667, 0.625, 0.609]	0.180
	AD ($\times 10^{-3}$)	1.155 (0.024)	1.163 (0.055) [1.225, 1.123, 1.140]	0.945

Data: mean (standard deviation), Data in [ ]: individual values for all subjects (Pediatric subjects: [subject 1, 2, 3, 4], Adult subjects: [subject 5, 6, 7]). * Corrected $p < 0.05$. Note b value for the pediatric controls and subject 1 was 1000 s/mm^2 whereas the b value for pediatric subjects 2, 3, and 4 as well as all adult subjects and adult controls was 700 s/mm^2.

Supplementary Table 2. Statistical results for the group comparisons of mean and variance of structural measures, network measures, and FA values of gyral connections and tracts of interest between pediatric and adult control groups

Control				
	Pediatric	**Adult**	***P*** (Mann-Whitney *U* test)	***P*** (Levene's test)
Structural measures				
Whole brain	1196374.0 (115682.5)	1304293.5 (70474.8)	0.027	0.172
Cortical gray matter	577592.9 (60720.8)	602590.6 (31327.9)	0.307	0.038
Cortical thickness	2.982 (0.282)	3.169 (0.101)	0.138	0.001*
Cortical surface area	167393.0 (21037.6)	166048.7 (8617.2)	0.249	0.049
White matter	395339.9 (58145.2)	450147.5 (32842.2)	0.016	0.164
Corpus callosum	3025.6 (473.5)	3343.2 (315.7)	0.052	0.387
Deep gray matter	49637.4 (5565.8)	53923.6 (4012.0)	0.06	0.734
Network measures				
Clustering coefficient	2.284 (0.135)	2.362 (0.219)	0.277	0.442
Transitivity	2.018 (0.099)	2.019 (0.192)	0.767	0.38
Characteristic path length	1.094 (0.018)	1.088 (0.018)	0.339	0.689
Global efficiency	0.947 (0.008)	0.950 (0.010)	0.41	0.502
Gyral neighbor connections				
1st	0.347 (0.010)	0.365 (0.020)	0.009*	0.479
2nd and 3rd	0.400 (0.009)	0.409 (0.021)	0.199	0.236
4th and higher	0.467 (0.018)	0.473 (0.022)	0.448	0.855

Manually Segmented Tracts				
CST.L	0.551 (0.027)	0.544 (0.028)	0.644	0.936
CST.R	0.547 (0.023)	0.551 (0.021)	0.717	0.531
ML.L	0.479 (0.024)	0.497 (0.023)	0.106	0.720
ML.R	0.483 (0.023)	0.502 (0.021)	0.093	0.552
CC	0.531 (0.014)	0.531 (0.026)	0.531	0.630
DLN.ant.L	0.419 (0.029)	0.438 (0.025)	0.249	0.982
DLN.ant.R	0.422 (0.029)	0.445 (0.022)	0.032	0.955
DLN.post.L	0.407 (0.025)	0.406 (0.035)	0.668	0.306
DLN.post.R	0.410 (0.035)	0.395 (0.047)	0.379	0.309
VLN.ILF.L	0.445 (0.031)	0.444 (0.041)	1.000	0.507
VLN.ILF.R	0.463 (0.031)	0.460 (0.044)	0.717	0.273
VLN.IFOF.L	0.473 (0.026)	0.474 (0.026)	0.974	0.929
VLN.IFOF.R	0.472 (0.037)	0.472 (0.036)	0.974	0.961
VLN.UF.L	0.371 (0.039)	0.388 (0.045)	0.307	0.879
VLN.UF.R	0.390 (0.019)	0.374 (0.041)	0.199	0.080
Cing.L	0.453 (0.033)	0.481 (0.037)	0.121	0.631
Cing.R	0.414 (0.039)	0.461 (0.039)	0.009	0.466

Data: mean (standard deviation)

* Corrected $p < 0.05$. False discovery rate (FDR) control was performed for each of 8 statistical test sets. L or R follow tract abbreviation denotes left or right, respectively.

Supplementary Table 3. Statistical results for the group comparisons of mean and variance of structural measures, network measures, and FA values of gyral connections and tracts of interest between pediatric and adult subjects in TUBB3 E410K group

TUBB3 E410K				
	Pediatric	**Adult**	***P*** (Mann-Whitney *U* test)	***P*** (Levene's test)
Structural measures				
Whole brain	1071493.5 (147653.2)	1034269.3 (151287.8)	1	0.997
Cortical gray matter	550616.9 (72825.1)	499428.3 (81908.6)	0.629	0.857
Cortical thickness	3.152 (0.120)	3.069 (0.195)	0.629	0.231
Cortical surface area	146488.0 (17087.4)	135289.7 (14226.1)	0.629	0.862
White matter	338966.8 (65491.6)	343225.8 (62153.8)	1	0.949
Corpus callosum	1576.2 (240.7)	1834.4 (224.5)	0.229	0.88
Deep gray matter	42818.8 (4429.5)	46690.6 (5421.6)	0.629	0.599
Network measures				
Clustering coefficient	2.810 (0.214)	3.018 (0.163)	0.229	0.291
Transitivity	2.389 (0.133)	2.473 (0.177)	0.629	0.713
Characteristic path length	1.131 (0.029)	1.129 (0.008)	1	0.028
Global efficiency	0.928 (0.013)	0.926 (0.004)	1	0.089
Gyral neighbor connections				
1st	0.329 (0.015)	0.360 (0.007)	0.057	0.273
2nd and 3rd	0.367 (0.014)	0.398 (0.010)	0.057	0.479

4th and higher	0.408 (0.017)	0.442 (0.016)	0.114	0.944
Manually Segmented Tracts				
CST.L	0.433 (0.023)	0.482 (0.027)	0.114	0.935
CST.R	0.400 (0.008)	0.422 (0.041)	0.629	0.013
ML.L	0.427 (0.006)	0.460 (0.042)	0.629	0.034
ML.R	0.402 (0.032)	0.417 (0.043)	0.629	0.466
CC	0.376 (0.044)	0.403 (0.003)	0.400	0.105
DLN.ant.L	0.368 (0.024)	0.375 (0.039)	1.000	0.443
DLN.ant.R	0.364 (0.014)	0.362 (0.021)	1.000	0.360
DLN.post.L	0.392 (0.009)	0.348 (0.080)	0.400	0.010
DLN.post.R	0.360 (0.017)	0.350 (0.069)	0.629	0.035
VLN.ILF.L	0.416 (0.033)	0.397 (0.019)	0.629	0.513
VLN.ILF.R	0.393 (0.043)	0.425 (0.031)	0.229	0.661
VLN.IFOF.L	0.375 (0.027)	0.395 (0.031)	0.629	0.836
VLN.IFOF.R	0.379 (0.024)	0.398 (0.034)	0.629	0.564
VLN.UF.L	0.319 (0.032)	0.357 (0.021)	0.267	0.533
VLN.UF.R	0.350 (0.060)	0.371 (0.060)	1.000	0.994
Cing.L	0.386 (0.038)	0.438 (0.017)	0.114	0.076
Cing.R	0.349 (0.046)	0.411 (0.011)	0.114	0.257

Data: mean (standard deviation). L or R follow tract abbreviation denotes left or right, respectively.

E. Supplementary References

Achenbach TM, Rescorla LA. 2001. Manual for the ASEBA School-Age Forms & Profiles. Burlington, VT: University of Vermont, Research Center for Children, Youth, & Families.

Beck AT, Steer RA, Brown GK. 1996. Manual for the Beck Depression Inventory-II. San Antonio, TX: Psychological Corporation.

Carrow-Woolfolk E. 1995. Oral and Written Language Scales (OWLS). Circle Pines, MN: American Guidance.

Catani M, Jones DK, ffytche DH. 2005. Perisylvian language networks of the human brain. Annals of neurology. 57:8-16.

Catani M, Thiebaut de Schotten M. 2008. A diffusion tensor imaging tractography atlas for virtual in vivo dissections. Cortex; a journal devoted to the study of the nervous system and behavior. 44:1105-1132.

Chorpita BF, Moffitt CE, Gray J. 2005. Psychometric properties of the Revised Child Anxiety and Depression Scale in a clinical sample. Behav Res Ther. 43:309-322.

Chorpita BF, Yim L, Moffitt C, Umemoto LA, Francis SE. 2000. Assessment of symptoms of DSM-IV anxiety and depression in children: a revised child anxiety and depression scale. Behav Res Ther. 38:835-855.

Conners KC. 2008. Conners Toronto, Ontario, Canada: Multi-Health Systems.

Constantino JN. 2002. Social Responsiveness Scale (SRS). Los Angeles, CA: Western Psychological Services.

Dick AS, Tremblay P. 2012. Beyond the arcuate fasciculus: consensus and controversy in the connectional anatomy of language. Brain : a journal of neurology. 135:3529-3550.

Forkel SJ, Thiebaut de Schotten M, Dell'Acqua F, Kalra L, Murphy DG, Williams SC, Catani M. 2014. Anatomical predictors of aphasia recovery: a tractography study of bilateral perisylvian language networks. Brain : a journal of neurology. 137:2027-2039.

Gioia GA, Isquith PK, Guy SC, Kenworthy L. 2000. Behavior Rating Inventory of Executive Function. Odessa, FL: Psychological Assessment Resources.

Harrison PL, Oakland T. 2003. Adaptive Behavior Assessment System San Antonio, TX: The Psychological Corporation.

Hau J, Sarubbo S, Perchey G, Crivello F, Zago L, Mellet E, Jobard G, Joliot M, Mazoyer BM, Tzourio-Mazoyer N, Petit L. 2016. Cortical Terminations of the Inferior Fronto-Occipital and Uncinate Fasciculi: Anatomical Stem-Based Virtual Dissection. Front Neuroanat. 10:58.

Kovacs M. 1992. Children's Depression Inventory (CDI). North Tonawanda, New York: Multi-Health Systems, Inc.

Le Couteur A, Rutter M, Lord C, Rios P, Robertson S, Holdgrafer M, McLennan J. 1989. Autism diagnostic interview: a standardized investigator-based instrument. Journal of autism and developmental disorders. 19:363-387.

Lord C, Risi S, Lambrecht L, Cook EH, Jr., Leventhal BL, DiLavore PC, Pickles A, Rutter M. 2000. The autism diagnostic observation schedule-generic: a standard measure of social and communication deficits associated with the spectrum of autism. Journal of autism and developmental disorders. 30:205-223.

Lord C, Rutter M, Le Couteur A. 1994. Autism Diagnostic Interview-Revised: a revised version of a diagnostic interview for caregivers of individuals with possible pervasive developmental disorders. Journal of autism and developmental disorders. 24:659-685.

March JS. 1997. Multidimensional Anxiety Scale for Children (MASC). North Tonawanda, NY: Multi-Health Systems, Inc.

Martino J, De Lucas EM. 2014. Subcortical anatomy of the lateral association fascicles of the brain: A review. Clin Anat. 27:563-569.

Mullen EM. 1995. Mullen Scales of Early Learning (AGS Edition). Circle Pines, MN: American Guidance.

Norton I, Essayed W, Zhang F, Pujol S, Yarmarkovich A, Golby AJ, Kindlmann G, Wassermann D, Estepar RSJ, Rathi Y, Pieper S, Kikinis R, Johnson HJ, Westin CF, O'Donnell LJ. 2017. SlicerDMRI: Open Source Diffusion MRI Software for Brain Cancer Research. Cancer Res. 77:e101-e103.

Roid GH. 2003. Stanford-Binet Intelligence Scales. Itasca, IL: Riverside Publishing.

Rutter M, Bailey A, Lord C. 2003. Social Communication Questionnaire (SCQ). Los Angeles, CA: Western Psychological Services.

Semel E, Wiig EH, Secord WA. 2003. Clinical Evaluation of Language Fundamentals [CELF-4]. San Antonio, TX: PsychCorp.

Sparrow S, Cicchetti D, Balla D. 2005. Vineland Adaptive Behavior Scales. Minneapolis, MN: Pearson Assessment.

Sparrow SS, Balla DA, Cicchetti DV. 1984. Vineland Adaptive Behavior Scales: Interview Edition, Survey Form Manual. Circle Pines, MN: American Guidance Service.

Swanson JM, Schuck S, Porter MM, Carlson C, Hartman CA, Sergeant JA, Clevenger W, Wasdell M, McCleary R, Lakes K, Wigal T. 2012. Categorical and Dimensional Definitions and Evaluations of Symptoms of ADHD: History of the SNAP and the SWAN Rating Scales. Int J Educ Psychol Assess. 10:51-70.

Wechsler D. 2003. Wechsler Intelligence Scale for Children (WISC-IV). San Antonio, TX: The Psychological Corporation.